

2 Spectroscopic Properties of Mixed-Valence Compounds in the Impurity Model

Kurt Schönhammer
Institut für Theoretische Physik
Universität Göttingen

Contents

1	Introduction	2
2	Basic impurity models	3
2.1	Spin-degenerate single-impurity Anderson model	3
2.2	Impurity models involving core levels	8
3	Anderson impurity model with large orbital degeneracy	8
3.1	Ground-state calculation	9
4	The intermediate states method for spectra	12
4.1	Valence photoemission spectroscopy	12
4.2	Inverse Photoemission	14
4.3	Spectra involving core holes	17
5	Comparison with experiment	18

1 Introduction

The electronic properties of mixed valence lanthanide materials, like Ce compounds, were studied experimentally over a long period of time. In addition to thermodynamic and transport measurements various “high energy” spectroscopies like valence photoemission, inverse photoemission, and core level spectroscopies were used to understand the electronic properties of the f -levels of such systems [1]. It took some time until it was realized that electronic correlations play an essential role for the understanding of the f -spectra. As a first step in the attempt at theoretical understanding, a single rare-earth atom in a simple metal can be studied using the single-impurity Anderson model [2]. In this model, discussed in detail in the following, the energy ε_f of the f -level, the coupling Δ to the conduction electrons, and the Coulomb repulsion U between two electrons in the f -level are the essential parameters that determine quantities like the total f -level occupancy n_f . If spin-orbit coupling and crystal-field splitting are neglected the degeneracy of the f -level is given by $N_f = 14$.

The f -electron spectral function of the Anderson impurity model was a long-standing issue. If the coupling Δ is weak, and the Fermi level falls between ε_f and $\varepsilon_f + U$, the spectrum has a peak near ε_f (seen in photoemission) and a peak near $\varepsilon_f + U$ (seen in inverse photoemission). It was further realized that the spectrum has resonance close to $\varepsilon_F = 0$ usually called the Kondo resonance [3, 4]. Except for some special cases [5] it was, however, for a long time hard to determine even the qualitative properties of the Kondo resonance.

A historically important progress in the treatment of the Anderson impurity model was the realization in the early eighties that $1/N_f$ can be treated as a small parameter [6, 7]. Using this idea O. Gunnarsson and the author developed a method for calculating zero-temperature spectral properties (*intermediate states method*), which becomes exact in the limit $N_f \rightarrow \infty$ [8–11]. In particular, this method makes it possible to study the Kondo peak quantitatively for large values of N_f . Analytical results in the infinite- U limit obtained to leading order in $1/N_f$ are presented in the following sections. Higher-order calculations that require numerical work usually converge quickly for $N_f = 14$. They were successfully used for a comparison to the experimental spectra of Ce compounds [9, 10, 12].

Apart from second quantization, the intermediate states method uses only basic quantum mechanics. The knowledge of more sophisticated many-body techniques, like Feynman diagrams, is not necessary to understand it. This is presumably one of the reasons why it is used frequently by experimental groups for the interpretation of their measured spectra.

At about the same time as the intermediate states method, large N_f approaches (for infinite U) were proposed that allow an extension to finite temperatures [13–16]. Some of the ideas in these papers can be traced back to earlier work [17, 18]. Using different many-body techniques, these approaches lead to the same set of integral equations in the so-called non-crossing approximation (NCA). Usual Feynman diagram techniques can be used in the derivation if a slave boson is introduced [16]. There is a chapter on the slave-boson technique in this book.

At the time of these developments Wilson's numerical renormalization group method (NRG) to calculate ground state properties of the spin-degenerate Anderson impurity model numerically to arbitrary accuracy was known [19], but the extension to calculate the impurity spectral function came more than ten years after Wilson's work [20,21]. There are two chapters on the NRG in this book. Therefore it is not further discussed here.

Later the NCA was generalized to finite values of U [22–24] and further improved [25, 26] to correctly obtain the Kondo scale for $N_f = 2$. Another approach that circumvents many of the earlier deficiencies in the treatment of the spin-degenerate single-impurity Anderson model (SIAM) is the *local moment approach* [27]. It was later extended to include orbital degeneracy [28].

Exact results for ground-state and thermodynamic properties of the spin-degenerate Anderson impurity model were presented using the Bethe ansatz [29, 30]. Later, this approach was extended to models with large orbital degeneracy in the limit $U \rightarrow \infty$ [31]. Unfortunately results for spectral properties by this method do not (yet) exist.

Additional motivation for simple accurate calculational schemes for the impurity spectral function came later from the development of the dynamical mean-field theory (DMFT) [32], in which an extended lattice model of correlated electrons is mapped onto a SIAM with a coupling to a bath whose structure has to be determined self-consistently. Then the coupling of the impurity to the conduction band can have an arbitrary energy dependence.

In section 2 the Anderson impurity model in its basic form as well as the minimal model for an impurity with a core level in a metal are introduced. Important new aspects arising when the orbital degeneracy is taken into account are discussed in section 3. As a first example of the ideas of the $1/N_f$ expansion presented in the following, the ground state of the impurity system is discussed. In section 4 the intermediate states method is introduced and applied to the description of various spectroscopies. The comparison with spectroscopic measurements of mixed-valence compounds is briefly addressed in section 5.

2 Basic impurity models

2.1 Spin-degenerate single-impurity Anderson model

In order to study a single magnetic impurity in simple metals, P.W. Anderson proposed the Hamiltonian [2]

$$H_A = \sum_{\sigma} \left[\varepsilon_d n_{d\sigma} + \sum_k \varepsilon_k n_{k\sigma} + \sum_k V_{dk} \left(\psi_{d\sigma}^{\dagger} \psi_{k\sigma} + H.c. \right) \right] + U n_{d\uparrow} n_{d\downarrow}, \quad (1)$$

where $\psi_{d,\sigma}$ is the annihilation operator of the localized impurity $|d\rangle$ -state with energy ε_d , and the $\psi_{k,\sigma}$ are the annihilation operators of the delocalized band states $|k\rangle$ with energy ε_k . The $n_{d\sigma} = \psi_{d\sigma}^{\dagger} \psi_{d\sigma}$ (and $d \rightarrow k$) are particle number operators. In the body of his 1961 paper Anderson used the “physically unrealistic case” with only spin degeneracy and treated the case

of a doubly degenerate d -orbital in an appendix [2]. As a “physically realistic” case the spin-degenerate model was later used to describe hydrogen chemisorption on metal surfaces ($d \rightarrow a$ for “adsorbate”), where $|a\rangle$ corresponds to the hydrogen $1s$ -level [33]. The last term of the Anderson Hamiltonian describes the local Coulomb repulsion U , which acts when the d -level is doubly occupied. This two-body interaction makes the model highly non-trivial.

Experimentally relevant spectral functions are obtained from the one-particle Green’s functions. The general definition of the retarded functions [34] is

$$\langle\langle A; B \rangle\rangle_z \equiv -i \int_0^\infty \langle [A(t), B]_\pm \rangle e^{izt} dt, \quad (2)$$

where $A(t) = e^{iHt} A e^{-iHt}$ is the operator A in the Heisenberg picture, $\langle \rangle$ denotes the average over the grand canonical ensemble, and z is a complex variable with $\text{Im } z > 0$ in order to ensure the convergence of the time integral. For operators A involving products of an odd (even) number of fermion field operators the anticommutator $[,]_+$ (commutator $[,]_-$) is chosen. The Heisenberg equation of motion (EOM) for $A(t)$ and a partial integration yields the EOM

$$z \langle\langle A; B \rangle\rangle_z - \langle\langle [A, H]; B \rangle\rangle_z = \langle [A, B]_\pm \rangle. \quad (3)$$

This EOM is very useful for discussing the exactly solvable limits of the Anderson impurity model.

The retarded one-particle Green’s functions $G_{ij}(z)$ is obtained by $A \rightarrow \psi_i, B \rightarrow \psi_j^\dagger$

$$G_{ij}(z) \equiv \langle\langle \psi_i; \psi_j^\dagger \rangle\rangle_z. \quad (4)$$

At zero temperature the local Green’s function takes the form

$$\begin{aligned} G_{d\sigma, d\sigma}(z) &\equiv \left\langle E_0(N) \left| \psi_{d\sigma}^\dagger \frac{1}{z + H - E_0(N)} \psi_{d\sigma} + \psi_{d\sigma} \frac{1}{z - H + E_0(N)} \psi_{d\sigma}^\dagger \right| E_0(N) \right\rangle \\ &\equiv G_{d\sigma, d\sigma}^<(z) + G_{d\sigma, d\sigma}^>(z). \end{aligned} \quad (5)$$

The first term is relevant for photoemission and the second one for inverse photoemission. At finite temperature T the spectral functions are obtained as

$$\rho_{dd}^<(\varepsilon) = -\frac{1}{\pi} f(\varepsilon) \text{Im } G_{d\sigma, d\sigma}(\varepsilon + i0) \text{ and } \rho_{dd}^>(\varepsilon) = -\frac{1}{\pi} (1 - f(\varepsilon)) \text{Im } G_{d\sigma, d\sigma}(\varepsilon + i0), \quad (6)$$

where $f(\varepsilon) = 1/(e^{\beta\varepsilon} + 1)$ is the Fermi function with $\beta = 1/k_B T$ and the chemical potential is chosen as the zero of energy. This leads to

$$\rho_{dd}^>(\varepsilon) = e^{\beta\varepsilon} \rho_{dd}^<(\varepsilon). \quad (7)$$

This relation can be read as “photoemission determines inverse photoemission.” It has been used in the present context to get information about a Kondo resonance above the chemical potential by means of photoemission [35]. Unfortunately the relation is of limited practical use.

For $U = 0$ the Anderson impurity model describes noninteracting electrons and is exactly solvable. The generally valid EOMs follow from Eq. (3)

$$(z - \varepsilon_d) G_{d\sigma, d\sigma}(z) - U \langle \langle \psi_{d\sigma} n_{d-\sigma}; \psi_{d\sigma}^\dagger \rangle \rangle_z - \sum_k V_{dk} G_{k\sigma, d\sigma}(z) = 1, \quad (8)$$

$$(z - \varepsilon_k) G_{k\sigma, d\sigma}(z) - V_{dk}^* G_{d\sigma, d\sigma}(z) = 0.$$

For $U = 0$ these equations close and one obtains

$$G_{d\sigma, d\sigma}^{U=0}(z) = \frac{1}{z - \varepsilon_d - \Gamma(z)}, \quad \text{with } \Gamma(z) = \sum_k \frac{|V_{dk}|^2}{z - \varepsilon_k}. \quad (9)$$

For finite systems $\Gamma(z)$ has poles on the real axis. In the thermodynamic limit they go over to a branch cut on the real axis.

Using $\rho_{d\sigma, d\sigma}(\varepsilon) = -\text{Im } G_{d\sigma, d\sigma}(\varepsilon + i0)/\pi$ one obtains the impurity spectral function. The only information about the band states that enters is the coupling function $\Gamma(\varepsilon + i0)$. It determines the width and location of the resonance resulting from the coupling. An often-used approximation for the coupling function is the wide-band limit $\Gamma(\varepsilon \pm i0) = \mp i\Gamma$ with a constant Γ . Then the $U = 0$ impurity spectral function $\rho_{d\sigma, d\sigma}(\varepsilon)$ has a Lorentzian peak of half-width Γ at ε_f . The mathematical structure of the results of the noninteracting limit of the Anderson model first appeared in earlier models by K.O. Friedrichs [36] and T.D. Lee [37].

A long history exists of attempts to solve the Anderson impurity model for finite values of the Coulomb interaction U . It started with Anderson using the Hartree-Fock (HF) approximation [2]

$$U n_{d\uparrow} n_{d\downarrow} \rightarrow U \left(n_{d\uparrow} \langle n_{d\downarrow} \rangle^{HF} + n_{d\downarrow} \langle n_{d\uparrow} \rangle^{HF} - \langle n_{d\uparrow} \rangle^{HF} \langle n_{d\downarrow} \rangle^{HF} \right), \quad (10)$$

which corresponds to a noninteracting model with the bare f -level position given by the replacement $\varepsilon_d \rightarrow \varepsilon_{d\sigma}^{HF} = \varepsilon_d + U \langle n_{d-\sigma} \rangle^{HF}$. This leads to

$$G_{d\sigma, d\sigma}^{HF}(z) = \frac{1}{z - \varepsilon_d - U \langle n_{d-\sigma} \rangle - \Gamma(z)}. \quad (11)$$

In the language of the EOMs the HF-approximation corresponds to the factorization of the retarded function $\langle \langle \psi_{d\sigma} n_{d-\sigma}; \psi_{d\sigma}^\dagger \rangle \rangle_z \rightarrow \langle n_{d-\sigma} \rangle \langle \langle \psi_{d\sigma}; \psi_{d\sigma}^\dagger \rangle \rangle_z$. The discussion of the results of the HF-approximation simplifies in the particle-hole-symmetric case $\varepsilon_d + U/2 = \mu = \varepsilon_F = 0$ for a symmetric band around the chemical potential. Then $\langle n_{d-\sigma} \rangle^{RHF} = 1/2 = \langle n_{d,-\sigma} \rangle^{exact}$ and the R(estricted)HF resonance is at the chemical potential. The shape and position of this RHF spectral function is *independent* of the value of U in this particle-hole symmetric case. At a critical value $U/\Gamma = \pi$ solutions of the HF-equations occur where the occupancies of the impurity level for spin-up and spin-down differ [2]. These ‘‘unrestricted Hartree-Fock’’ (UHF) solutions are an artifact of the approximation as no spontaneous symmetry breaking can occur when the interaction acts in a zero dimensional system. Therefore the spin variable in the Green’s function is suppressed in (most of) the following (e.g. $d\sigma \rightarrow d$).

In order to properly describe the U -dependence of G_{dd} , a better treatment of the self-energy $\Sigma(z)$ defined in the usual way

$$G_{dd}(z) = \frac{1}{z - \varepsilon_d - \Gamma(z) - \Sigma(z)} \quad (12)$$

is necessary. The first order contribution in U to the self-energy Σ is just the HF-term $U\langle n_{d,-\sigma} \rangle$. In the particle-hole symmetric case and the wide-band limit the spectral function takes the form ($\tilde{\Sigma} \equiv \Sigma - U\langle n_{d,-\sigma} \rangle$)

$$\rho_{dd}(\varepsilon) = \frac{1}{\pi} \frac{\Gamma + |\text{Im}\tilde{\Sigma}(\varepsilon + i0)|}{\left(\varepsilon - \text{Re}\tilde{\Sigma}(\varepsilon)\right)^2 + \left(\Gamma + |\text{Im}\tilde{\Sigma}(\varepsilon + i0)|\right)^2} \quad (13)$$

with $\text{Re}\tilde{\Sigma}(\varepsilon)$ an even function of ε . At zero temperature the Fermi liquid property holds: $\text{Im}\tilde{\Sigma}(\varepsilon + i0) \sim \varepsilon^2$ for $\varepsilon \rightarrow 0$. This can be seen easily for the self-energy to second order in U and has been discussed to arbitrary order by Yamada and Yoshida [38]. This implies the exact result for the particle-hole symmetric case at $T = 0$:

$$\rho_{dd}(0) = \rho_{dd}^{RHF}(0) = \frac{1}{\pi\Gamma}. \quad (14)$$

Important additional insights into the energy dependence of $\rho_{dd}(\varepsilon)$ are obtained by considering the exactly solvable *atomic limit*, in which $V_{dk} = 0$ for all values of k . Again the EOMs close, as $(z - \varepsilon_d - U)\langle\langle\psi_{d\sigma}n_{d-\sigma}; \psi_{d\sigma}^\dagger\rangle\rangle_z = \langle n_{d-\sigma} \rangle$ holds for vanishing coupling to the conduction band. Keeping the spin indices one obtains

$$G_{d\sigma,d\sigma}^{V=0}(z) = \frac{1 - \langle n_{d-\sigma} \rangle}{z - \varepsilon_d} + \frac{\langle n_{d-\sigma} \rangle}{z - (\varepsilon_d + U)}. \quad (15)$$

Here we only discuss the most interesting case when ε_d is below the Fermi energy and $\varepsilon_d + U$ is above it. Then the total occupancy of the impurity level is approximately one, which holds exactly in the particle-hole symmetric case. If an electron is removed from the impurity level the empty impurity state created can decay by the tunneling back in of a spin-up *or* spin-down electron, which gives the ‘‘atomic peaks’’ a width *twice* as large as the width of the RHF-Lorentzian:

$$G_{dd}(z) \approx \frac{1/2}{z - U/2 - 2\Gamma(z)} + \frac{1/2}{z + U/2 - 2\Gamma(z)}. \quad (16)$$

A formal way to obtain this result is to calculate a properly defined self-energy matrix to second order in the hybridization V [39]. For $U \gg \Gamma$ most of the spectral weight is in the atomic peaks that are assumed to be well described. At the chemical potential, the spectral weight vanishes in this large- U limit as $\sim \Gamma/U^2$ instead of yielding the exact result $1/(\pi\Gamma)$. This implies that a very narrow peak at the Fermi energy is missing.

Both approximations for the local spectral function in the particle-hole symmetric case presented so far are unable to properly describe this *Kondo resonance* at the Fermi energy. An exact (numerical) calculation was only presented in the eighties with the help of the numerical renormalization group (NRG) [20]. The exact NRG result in the wide band limit for $U/\Gamma = 4\pi$ is shown in Fig. 1. The RHF result agrees with the exact NRG result only for $\varepsilon = 0$ but otherwise fails badly. The naive perturbation theory around the atomic limit fails badly in the low energy region. For larger values of U/Γ than shown in Fig. 1 the high energy features near $\pm U/2$ agree better with the NRG-result.

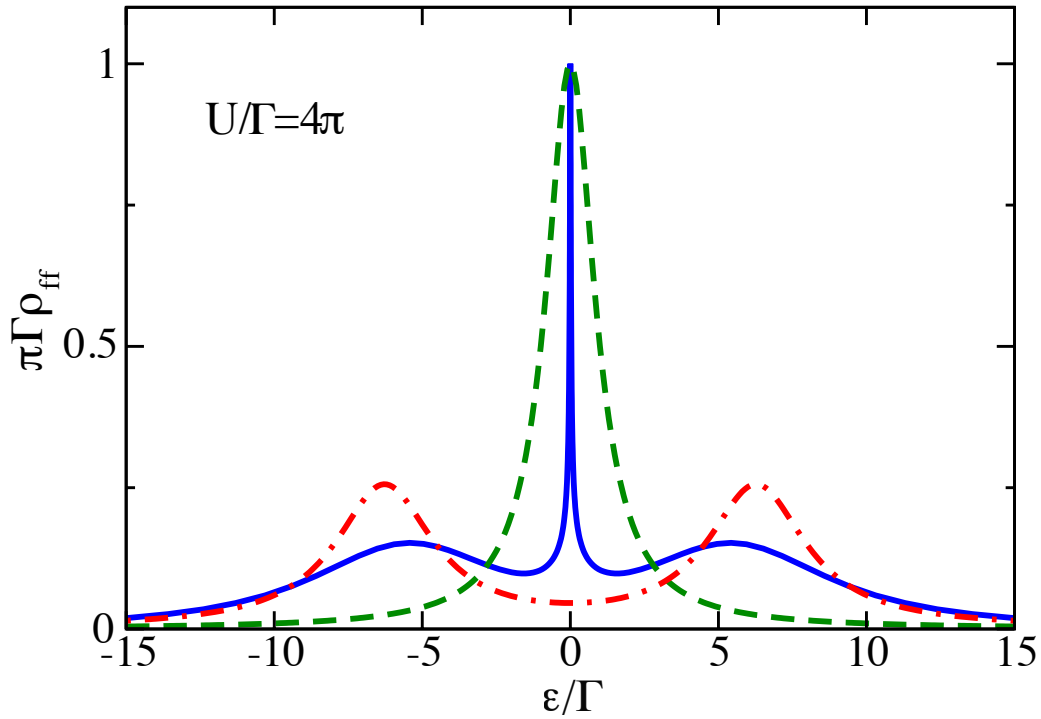


Fig. 1: Result for the impurity spectral function of the spin-symmetric Anderson model in the particle-hole symmetric case in the wide band limit for $U/\Gamma = 4\pi$: exact result from the numerical renormalization group (NRG) with the Kondo peak at the Fermi energy (full line); restricted Hartree-Fock approximation (dashed line); perturbation theory around the atomic limit (dashed-dotted line)

The simple arguments presented in favor of the Kondo resonance in the particle-hole symmetric case give no information about its width and its precise location if $|\varepsilon_d| \neq |\varepsilon_d + U|$. Before the NRG results were available, it was therefore useful to obtain partial answers to these questions in the limit of large additional orbital degeneracy of the impurity level. This is discussed in detail in the following sections.

There is a long history of attempts to obtain a controlled approximation for G_{dd} and the corresponding spectral function that cannot be presented here in detail. We shortly mention decoupling schemes of higher order Green's functions that appear in the EOM of $\langle\langle\psi_{d\sigma}n_{d-\sigma};\psi_{d\sigma}^\dagger\rangle\rangle_z$ or in the EOMs of higher order [40–44]. The quality of the results for G_{dd} is generally hard to judge. The resulting spectral functions can have frequency regions with *negative* spectral weight [43]. Special attention to the large N_f limit has been given by Czycholl [44]. To leading order in $1/N_f$, he obtains at zero temperature a sharp peak at the correct Kondo energy.

Additional information on the attempts to understand the physics of the SIAM can be found in the book by A. Hewson [45].

2.2 Impurity models involving core levels

X-ray absorption spectroscopy and X-ray photoemission spectroscopy (XPS) of the core levels of an impurity are useful tools for obtaining information about the properties of the valence electrons. In a minimal model, a single nondegenerate core level of the impurity with energy ε_c is considered, which is filled in the initial state. The creation of the core hole in the photoemission process leads to an additional attractive potential for the valence level of the impurity which lowers it by an amount U_{dc} . The corresponding model Hamiltonian reads

$$H_{tot} = H_A + \varepsilon_c n_c - U_{dc}(1 - n_c) \sum_{\sigma} n_{d\sigma}. \quad (17)$$

As the ground state of the combined system has the form $\psi_c^\dagger |E_0(N)\rangle$, with $|E_0(N)\rangle$ the ground state of the valence system with the core hole present, the time evolution of the remaining pure valence system after removing the core electron is described by the modified Anderson Hamiltonian \tilde{H}_A , with the energy ε_d of the impurity level replaced by $\varepsilon_d - U_{dc}$. The creation of the core hole acts as a *quantum quench* for the valence system. The core spectral function is

$$\rho_{cc}(\varepsilon) = \left\langle E_0(N) \left| \delta(\varepsilon - \varepsilon_c - E_0(N) + \tilde{H}_A) \right| E_0(N) \right\rangle. \quad (18)$$

For the case of *noninteracting* valence electrons, i.e., $U = 0$ in Eq. (1), this problem falls into the class of the famous X-ray edge singularity problem [46]. The sharp core-level spectrum without the presence of the valence electrons is replaced by a continuum with a *power law singularity* at the high-energy edge. This is closely related to the Anderson orthogonality catastrophe [47] which states that the overlap of the ground states of H_A and \tilde{H}_A vanishes with a power law in $1/N$ when the number of electrons N tends to infinity. The core-level spectrum can show satellite peaks corresponding to higher-energy eigenstates of \tilde{H}_A due to physical processes that occur on a *finite* time scale [48–50]. This has been addressed in detail, e.g., for core levels of adsorbates at metal surfaces [50]. For small coupling Γ a high energy resonance dominates the core level spectrum if the adsorbate level, initially well above the chemical potential, is pulled well below it when the core hole is created. For finite Coulomb interaction U , the problem cannot be solved exactly, and various approximations were proposed [51, 52]. The treatment within the large-degeneracy limit is discussed in section 4.

3 Anderson impurity model with large orbital degeneracy

Despite the fact that Anderson proposed his model to treat transition-metal impurities in simple metals, the five-fold orbital degeneracy of d -orbitals was not treated explicitly. The degeneracy of f -orbitals is given by $N_f = 14$ if spin degeneracy is included and spin-orbit coupling and crystal-field splitting is neglected. As mentioned in the introduction, an important progress in the treatment of the Anderson model was the realization that the treatment of $1/N_f$ as a small parameter allows new approximation schemes [6, 7]. In the SIAM Hamiltonian, Eq. (1), the

non-degenerate orbital label d is replaced by the orbital quantum number m and V_{kd} by V_{km} . We assume that in the thermodynamic limit

$$\sum_k V_{km}^* V_{km'} \delta(\varepsilon - \varepsilon_k) = V(\varepsilon)^2 \delta_{mm'} \quad (19)$$

holds [9, 10]. It is useful to introduce new one-particle states

$$|\varepsilon, m\sigma\rangle \equiv V(\varepsilon)^{-1} \sum_k V_{km} \delta(\varepsilon - \varepsilon_k) \quad (20)$$

and to use the combined degeneracy index $\nu \equiv m\sigma$. The orthogonality relation of these states reads $\langle \varepsilon, \nu | \varepsilon', \nu' \rangle = \delta_{\nu\nu'} \delta(\varepsilon - \varepsilon')$.

Despite the fact that it is mathematically more appropriate to write down the many-body Hamiltonian for finite systems and take the thermodynamic limit in the end of the calculation, in the following we formally write it down using creation and annihilation operators of the states defined in Eq. (20). To avoid problems, one can discretize the energies ε and replace the Dirac delta functions $\delta(\varepsilon - \varepsilon')$ by Kronecker deltas $\delta_{\varepsilon\varepsilon'}$. This is done anyway in the higher order numerical treatment of the $1/N_f$ scheme presented in the following sections [9]. Alternatively, one has to subtract the (infinite) energy of the filled Fermi sea.

Keeping these precautions in mind, the N_f -fold-degenerate single-impurity Anderson Hamiltonian used in the following reads

$$H = \sum_{\nu=1}^{N_f} \left[\varepsilon_f \psi_{\nu}^{\dagger} \psi_{\nu} + \int \varepsilon \psi_{\nu\varepsilon}^{\dagger} \psi_{\nu\varepsilon} d\varepsilon + \int (V(\varepsilon) \psi_{\nu}^{\dagger} \psi_{\nu\varepsilon} + H.c.) d\varepsilon \right] + U \sum_{\nu < \mu} n_{\nu} n_{\mu}. \quad (21)$$

The Hamiltonian \tilde{H}_0 , which contains linear combinations of conduction states that do not couple to the f -level, is not included. It can be neglected for the properties studied here.

As in the following $V(\varepsilon)$ enters in the combinations $N_f V(\varepsilon)^2$ and $V(\varepsilon)^2$, it is useful to define

$$\tilde{V}(\varepsilon) \equiv \sqrt{N_f} V(\varepsilon) \quad (22)$$

and require that $\tilde{V}(\varepsilon)$ is *independent* of the degeneracy N_f . This simplifies the discussion of the large degeneracy limit $N_f \rightarrow \infty$.

3.1 Ground-state calculation

The ground-state calculation is performed variationally by classifying the many-electron states shown in Fig. 2 in orders of $1/N_f$.

In the state $|0\rangle$, all conduction states below the Fermi energy are filled, and the f -level is empty. This state couples via H to the states denoted a in Fig. 2. They are of the form

$$|\varepsilon\rangle = \frac{1}{\sqrt{N_f}} \sum_{\nu} \psi_{\nu}^{\dagger} \psi_{\nu\varepsilon} |0\rangle \quad (23)$$

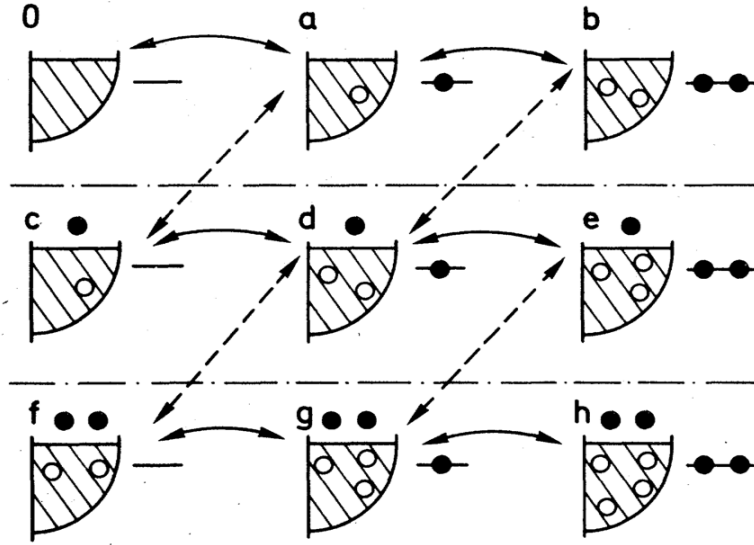


Fig. 2: Schematic representation of the many-electron basis states. Solid circles show electrons and open circles show holes. The hatched part indicates the filled conduction bands and the horizontal lines the f -level. The arrows show which states couple to each other. A solid line indicates the strength \tilde{V} and a dashed line the strength $\tilde{V}/\sqrt{N_f}$.

in which a conduction electron has hopped into the f -level. These states couple to the b states with two electrons in the f -level

$$|\varepsilon, \varepsilon'\rangle = \frac{1}{\sqrt{N_f(N_f - 1)}} \sum_{\nu \neq \nu'} \psi_\nu^\dagger \psi_{\varepsilon\nu} \psi_{\nu'}^\dagger \psi_{\varepsilon'\nu'} |0\rangle, \quad (24)$$

and to the c states with a conduction electron-conduction hole pair

$$|E\varepsilon\rangle = \frac{1}{\sqrt{N_f}} \sum_{\nu} \psi_{E\nu}^\dagger \psi_{\varepsilon\nu} |0\rangle, \quad (25)$$

where E refers to a conduction electron state above the Fermi level ($E > \varepsilon_F$). Further states in Fig. 2 can easily be written down [10].

The matrix elements coupling these states are given by

$$\langle \varepsilon | H | 0 \rangle = \tilde{V}(\varepsilon), \quad (26)$$

$$\langle \varepsilon, \varepsilon' | H | \varepsilon'' \rangle = \sqrt{1 - 1/N_f} \left(\tilde{V}(\varepsilon') \delta(\varepsilon - \varepsilon'') + \tilde{V}(\varepsilon) \delta(\varepsilon' - \varepsilon'') \right), \quad (27)$$

$$\langle E\varepsilon | H | \varepsilon' \rangle = \tilde{V}(E)/\sqrt{N_f} \delta(\varepsilon - \varepsilon'). \quad (28)$$

These examples illustrate the general result that within each row in Fig. 2 there are states that couple with strength \tilde{V} , while states in different rows at most couple with a strength $\tilde{V}/\sqrt{N_f}$. This allows one to classify the states in orders of $1/N_f$ according to their contribution to the ground state. The states in the first, second and third rows are of the orders $(1/N_f)^0$, $(1/N_f)^1$ and $(1/N_f)^2$, respectively.

As an illustration, we calculate the ground state for $U = \infty$ to lowest order in $1/N_f$. It is written as [53]

$$|E_0\rangle^{(0)} = A \left[|0\rangle + \int_{-B}^0 d\varepsilon a(\varepsilon) |\varepsilon\rangle \right], \quad (29)$$

where the normalization constant A is related to the total occupancy n_f of the f -level by $A^2 = 1 - n_f$. In contrast to the ground-state energy $E_0^{(0)}$, the difference $\Delta E_0 \equiv E_0^{(0)} - \langle 0|H|0\rangle$ is finite also in the thermodynamic limit. Using the coupling matrix elements Eq. (26) and $\langle \varepsilon|(H - \langle 0|H|0\rangle)|\varepsilon'\rangle = (\varepsilon_f - \varepsilon)\delta(\varepsilon - \varepsilon')$, the Schrödinger equation leads to

$$\Delta E_0 = \int_{-B}^0 \tilde{V}(\varepsilon) a(\varepsilon) d\varepsilon \quad \text{and} \quad (\Delta E_0 - \varepsilon_f + \varepsilon) a(\varepsilon) = \tilde{V}(\varepsilon). \quad (30)$$

Therefore ΔE_0 obeys the implicit equation

$$\Delta E_0 = \int_{-B}^0 \frac{\tilde{V}(\varepsilon)^2}{\Delta E_0 - \varepsilon_f + \varepsilon} d\varepsilon \rightarrow \tilde{V}^2 \ln \frac{\varepsilon_f - \Delta E_0}{\varepsilon_f - \Delta E_0 + B}, \quad (31)$$

where the energy integration was performed for the case of an energy-independent \tilde{V} . We discuss the solution for the case of constant \tilde{V} and ε_f well below the Fermi energy. Defining the (positive) $\delta \equiv \varepsilon_f - \Delta E_0$, $\tilde{\Delta} \equiv \pi \tilde{V}^2$, and $\tilde{\varepsilon}_f \equiv \varepsilon_f + (\tilde{\Delta}/\pi) \ln(\pi B/\tilde{\Delta})$ the equation for δ simplifies in the Kondo-limit $-\tilde{\varepsilon}_f \gg \tilde{\Delta}$ to

$$\delta = \frac{\tilde{\Delta}}{\pi} e^{\pi(\tilde{\varepsilon}_f - \delta)/\tilde{\Delta}} \rightarrow \delta \approx \frac{\tilde{\Delta}}{\pi} e^{\pi\tilde{\varepsilon}_f/\tilde{\Delta}}. \quad (32)$$

The coefficient

$$a(\varepsilon)^2 = \frac{\tilde{\Delta}}{\pi} \frac{1}{(\varepsilon - \delta)^2} \quad (33)$$

grows on the energy scale δ as the Fermi energy is approached from below. The total f -occupancy is determined by $\int a(\varepsilon)^2 d\varepsilon$. For the case of an energy-independent \tilde{V} , one obtains $n_f = \tilde{\Delta}/(\tilde{\Delta} + \pi\delta)$ [9]. The energy scale δ depends *exponentially* on $\pi\tilde{\varepsilon}_f/\tilde{\Delta}$, which suggests that it can be, apart from a factor given by the Boltzmann constant k_B , interpreted as the *Kondo temperature*: $T_K = k_B\delta$. This will be further examined in the following sections.

The infinite- U , lowest-order calculation presented above can be extended to the case when the spin-orbit splitting $\Delta\varepsilon_f$ is taken into account [9]. The single f -level (with $N_f = 14$) is replaced by two levels (with $N_{f_1} = 6$ and $N_{f_2} = 8$ for $j = 5/2$ and $j = 7/2$) at ε_f and $\varepsilon_f + \Delta\varepsilon_f$. For the description of high-resolution experimental spectra of Ce compounds it is important to include the spin-orbit splitting [54, 55].

The $(1/N_f)^0$ calculation of the ground state can also be extended to the *finite* U case. If an infinite three-body interaction is assumed, one just has to take the b states in Fig. 2 into account with an additional term with coefficients $b(\varepsilon, \varepsilon')$ in Eq. (29). The Schrödinger equation then leads to an integral equation for $a(\varepsilon)$ that for $U \gg B$ is of separable form [11]. For a detailed discussion of the explicit bandwidth behavior of the energy difference $\delta(U)$ between the nonmagnetic ground state and the lowest magnetic states that are not totally symmetric in the degeneracy indices, see Ref. [11].

Numerical ground-state calculations of higher order in $1/N_f$ using the states shown in Fig. 2 quickly converge for $N_f = 14$ [9, 10].

4 The intermediate states method for spectra

The theoretical description of photoemission simplifies considerably when the emitted electron in the state $|\kappa\rangle$ is assumed to have no interaction with the remaining $(N - 1)$ -electron system. This *sudden approximation* becomes increasingly accurate as the kinetic energy of the emitted electron is increased. In this approximation the photoelectron current can be calculated using Fermi's golden rule. For a weak energy dependence of the matrix elements $\tau_{\kappa i}$ of the dipole operator, where $|i\rangle$ is a valence state, the current is directly related to the spectral function of one-particle Green' functions $G_{ii}^<$ when interference effects are neglected [56, 10].

In Eq. (5) the zero-temperature local one-particle Green's functions $G^<$ and $G^>$ are expressed as an expectation value of the resolvent of the many body Hamiltonian H . One obtains the well known Lehmann representation by inserting the complete set of $(N \mp 1)$ -electron eigenstates of H . For $G^<$ one can alternatively use the resolution of unity made of an arbitrary complete set $\{|i\rangle\}$ of $(N - 1)$ -electron basis states

$$G_{\nu\nu}^<(z) = \sum_{ij} \langle E_0(N) | \psi_{\nu}^{\dagger} | i \rangle \langle i | (z + H - E_0(N))^{-1} | j \rangle \langle j | \psi_{\nu} | E_0(N) \rangle . \quad (34)$$

The inversion of the matrix $\tilde{H}(z)_{ij} \equiv \langle i | (z + H - E_0(N)) | j \rangle$ would lead to the exact result for $G_{\nu\nu}^<(z)$

$$G_{\nu\nu}^<(z) = \sum_{ij} \langle E_0(N) | \psi_{\nu}^{\dagger} | i \rangle (\tilde{H}(z)^{-1})_{ij} \langle j | \psi_{\nu} | E_0(N) \rangle \quad (35)$$

if the procedure could actually be carried out for a complete set of states. Approximations can be obtained by truncating the set $\{|i\rangle\}$ of *intermediate states*. Useful results can be obtained again using a classification of the states according to their contribution in orders of $1/N_f$. For the calculation of $G^>$ one can proceed the same way but with $(N + 1)$ -electron intermediate states $\{|i\rangle\}$.

4.1 Valence photoemission spectroscopy

Again, we first consider the $U = \infty$ case and work to lowest order in $1/N_f$. Then the ground state is described by Eq. (29). As $\psi_{\nu} | E_0 \rangle^{(0)} = A \int d\varepsilon a(\varepsilon) \psi_{\varepsilon\nu} | 0 \rangle / \sqrt{N_f}$, we introduce the basis states $|\varepsilon\nu\rangle$ which via H couple to the states $|\varepsilon\varepsilon'\nu\rangle$, where

$$|\varepsilon\nu\rangle \equiv \psi_{\varepsilon\nu} | 0 \rangle, \quad |\varepsilon\varepsilon'\nu\rangle \equiv \frac{1}{\sqrt{N_f}} \sum_{\nu'} \psi_{\nu'}^{\dagger} \psi_{\varepsilon'\nu'} \psi_{\varepsilon\nu} | 0 \rangle . \quad (36)$$

The matrix $\tilde{H}(z)$ defined before Eq. (35) has the matrix elements

$$\tilde{H}(z)_{\varepsilon,\varepsilon'} = (z - \Delta E_0 - \varepsilon) \delta(\varepsilon - \varepsilon'), \quad (37)$$

$$\tilde{H}(z)_{\varepsilon\varepsilon',\varepsilon''} = \tilde{V}(\varepsilon') \delta(\varepsilon - \varepsilon'') - \tilde{V}(\varepsilon) / \sqrt{N_f} \delta(\varepsilon' - \varepsilon''), \quad (38)$$

$$\tilde{H}(z)_{\varepsilon\varepsilon',\varepsilon_1\varepsilon_2} = (z - \Delta E_0 + \varepsilon_f - \varepsilon - \varepsilon') \delta(\varepsilon - \varepsilon_1) \delta(\varepsilon - \varepsilon_2) . \quad (39)$$

In leading order we neglect the term $\sim 1/\sqrt{N_f}$ on the right-hand side of the second equation. This leads to the simplification that for each $|\varepsilon\nu\rangle$ one can treat the coupling of this state to a continuum of states with an additional hole at $\varepsilon' < \varepsilon_F = 0$ separately. This greatly simplifies the leading-order calculation of $G_{\nu\nu}^<$.

For the inversion of $\tilde{H}(z)$, it is convenient to use a block matrix form with elements \tilde{H}_{11} , \tilde{H}_{12} , \tilde{H}_{21} and \tilde{H}_{22} , where e.g. \tilde{H}_{11} refers to the $\tilde{H}(z)_{\varepsilon,\varepsilon'}$ and \tilde{H}_{22} to $\tilde{H}(z)_{\varepsilon\varepsilon',\varepsilon_1\varepsilon_2}$. The well known matrix inversion formula

$$\left(\tilde{H}^{-1}\right)_{11} = \left(\tilde{H}_{11} - \tilde{H}_{12}\tilde{H}_{22}^{-1}\tilde{H}_{21}\right)^{-1} \quad (40)$$

simplifies the calculation. Since \tilde{H}_{22} is diagonal its inversion is trivial and one obtains

$$\left(\tilde{H}(z)^{-1}\right)_{\varepsilon\varepsilon'} = \tilde{g}(z - \Delta E_0 + \varepsilon_f - \varepsilon)\delta(\varepsilon - \varepsilon'), \quad (41)$$

where

$$\tilde{g}(z) = \frac{1}{z - \varepsilon_f - \tilde{\Gamma}(z)} \quad \text{with} \quad \tilde{\Gamma}(z) = \int_{-B}^0 \frac{\tilde{V}(\varepsilon)^2}{z - \varepsilon} d\varepsilon. \quad (42)$$

Note that the energy integration in the definition of $\tilde{\Gamma}(z)$ only extends to $\varepsilon_F = 0$. The function $\tilde{g}(z)$ has the form of the f Green's function of a noninteracting Anderson model with a sharp band cut-off at $\varepsilon = 0$. Finally, performing one of the energy integrations with the help of the delta function in Eq. (41), one obtains for $G_f^<$ to leading order in $1/N_f$

$$G_{\nu\nu}^<(z) = \frac{1}{N_f} A^2 \int_{-B}^0 a(\varepsilon')^2 \tilde{g}(z - \Delta E_0 + \varepsilon_f - \varepsilon') d\varepsilon'. \quad (43)$$

The function $\text{Im} \tilde{g}(\varepsilon \pm i0)$ has a continuum part for $-B \leq \varepsilon \leq 0$ due to the imaginary part of $\tilde{\Gamma}(\varepsilon \pm i0)$. As the transcendental equation (31) for $\Delta E_0^{(0)}$ can be written as $\Delta E_0 = -\tilde{\Gamma}(\delta)$, the function $\tilde{g}(z)$ has a pole at $z = \delta = \varepsilon_f - \Delta E_0$. The strength of the pole $(1 - d\tilde{\Gamma}/dz)^{-1}$ evaluated at $z = \delta$ is given by $1 - n_f$. This pole of \tilde{g} yields for the total f spectral function $\rho_f^<(\varepsilon) = -\sum_{\nu} \text{Im} G_{\nu\nu}^<(\varepsilon + i0)/\pi$ using Eq. (33) and $A^2 = 1 - n_f$ the expression

$$\rho_f^<(\varepsilon) = \frac{(1 - n_f)^2 \tilde{V}(\varepsilon)^2}{(\delta - \varepsilon)^2} \quad \text{for} \quad -\delta \leq \varepsilon \leq 0. \quad (44)$$

There is also a (partial) contribution of this type to $\rho_f^<(\varepsilon)$ for $-B \leq \varepsilon \leq \delta$. As $A^2 \int a(\varepsilon)^2 d\varepsilon = n_f$, the total weight of $\rho_f^<$ resulting from the pole of $\tilde{g}(z)$ at $z = \delta$ is given by $n_f(1 - n_f)$. It becomes very small in the Kondo limit $n_f \approx 1$.

For $\varepsilon < -\delta$ the continuum part of $\text{Im} \tilde{g}(\varepsilon \pm i0)$ also contributes to $\rho_f^<(\varepsilon)$, and there can be a split-off state below the conduction band in $\tilde{g}(z)$.

The low-energy spectral weight described in Eq. (44) rises sharply as ε approaches $\varepsilon_F = 0$ from below. It is the tail of the Kondo resonance present at $\varepsilon \approx \delta$ in the spectral function $\rho_f^>(\varepsilon)$ describing *inverse* photoemission. This is discussed in the next subsection. This low-energy behavior is totally different from the noninteracting case for $N_f = 1$. When ε_f lies below the Fermi energy, the f -spectral density in the $N_f = 1$ case has an ionization peak near ε_f and the spectral density *decreases* when ε approaches $\varepsilon_F = 0$ from below. In the Kondo limit

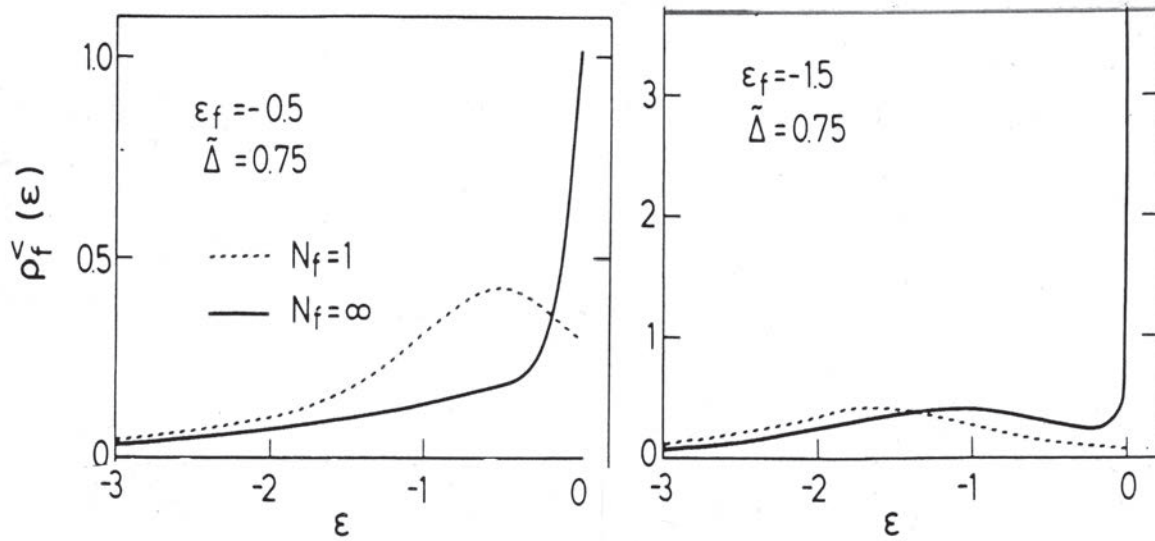


Fig. 3: Comparison of the leading order result for $\rho_f^<(\varepsilon)$ (full lines) with the result of a $N_f = 1$ calculation where Δ is replaced by $\tilde{\Delta}$ (dotted lines) for two different values of ε_f .

$-\varepsilon_f \gg \tilde{\Delta}$, implying $n_f \approx 1$, a similar ionization peak near ε_f dominates $\rho_f^>(\varepsilon)$. In this limit the energy integration with $A^2 a(\varepsilon')^2$ in Eq. (43) for $-\varepsilon \gg \delta$ approximately acts like (one-sided) delta function at the origin and $\rho_f^<(\varepsilon) \approx -\text{Im} \tilde{g}(\varepsilon + i0)/\pi$ holds. The width of this peak is given by $\tilde{\Delta} = N_f \Delta$, where $\Delta = \pi V^2(\varepsilon_f)$ is the half-width of the model for $N_f = 1$. After removing an f -electron from the ground state given by Eq. (29), the probability that a conduction electron in channel ν with energy $\varepsilon \approx \varepsilon_f$ hops into the f -level is given by Δ . Since there are N_f such channels the width is given by $N_f \Delta = \tilde{\Delta}$.

In Fig. 3, we compare results for the leading order result of $\rho_f^>(\varepsilon)$ with the result of a $N_f = 1$ calculation where Δ is replaced by $\tilde{\Delta}$. For both cases shown ε_f is below the Fermi level. In the left part of the figure $|\varepsilon_f| < \tilde{\Delta}$ and the ionization peak of the $N_f = 1$ spectrum only shows as a shoulder in the leading-order result for $\rho_f^>(\varepsilon)$. In the right half of the figure $|\varepsilon_f| = 2\Delta$ and the ionization peak is more asymmetric than the $N_f = 1$ result. This is similar to Fig. 1 where in the exact NRG result the atomic peaks are more asymmetric than the result from simple perturbation theory around the atomic limit.

The leading order calculation of $G_{\nu\nu}^<(z)$ can again be extended to the case of including spin-orbit splitting [9] and the case of finite U [11].

4.2 Inverse Photoemission

In inverse photoemission, earlier called Bremsstrahlung isochromat spectroscopy (BIS), the sample is bombarded by electrons that make radiative transitions into lower-lying $(N + 1)$ -electron states. Here we discuss transitions into the f -level. The theoretical description is in terms of

$$G_{\nu\nu}^>(z) = \left\langle E_0(N) \left| \psi_\nu \frac{1}{z - H + E_0(N)} \psi_\nu^\dagger \right| E_0(N) \right\rangle. \quad (45)$$

As the integrated weight of the total spectral function $\rho_{\nu\nu} = \rho_{\nu\nu}^< + \rho_{\nu\nu}^>$ is unity and $\int \rho_{\nu\nu}^<(\varepsilon) d\varepsilon = n_f/N_f$ holds, with $n_f \leq 1$ in the infinite U case, the integrated weight of $\rho_{\nu\nu}^>$ is given by $1 - n_f/N_f$, i.e., it is larger by a factor of N_f than the integrated weight of $\rho_{\nu\nu}^<$. This is a clear hint that a $1/N_f$ approximation for the full $G_{\nu\nu}$ is problematic. If it does not fulfill $\rho_{\nu\nu}^<(0) = \rho_{\nu\nu}^>(0)$, which is expected for an exact description at any finite N_f , this is an indication of the requirement to treat $G_{\nu\nu}^>$ differently from $G_{\nu\nu}^<$.

If in Eq. (45) the ground state to leading order in $1/N_f$ Eq. (29) is used, one has to calculate the expectation value of the resolvent of the many-body Hamiltonian with

$$\psi_{\nu}^{\dagger}|E_0\rangle^{(0)} = A \left[\psi_{\nu}^{\dagger}|0\rangle + \frac{1}{\sqrt{N_f}} \sum_{\nu'(\neq\nu)} \int d\varepsilon a(\varepsilon) \psi_{\nu}^{\dagger}\psi_{\nu'}^{\dagger}\psi_{\varepsilon\nu'}|0\rangle \right]. \quad (46)$$

In the first state on the right-hand side the f -level is singly occupied (f^1), while in the states in the second term it is doubly occupied (f^2). Integrating the corresponding expectation values of $\delta(\varepsilon - H + E_0(N))$ shows that the total weight of the f^1 contribution is given by $1 - n_f$ and the f^2 weight by $n_f(1 - 1/N_f)$. For large values of U the two different contribution are energetically well separated.

In a first attempt, one would take the states on the right-hand side of Eq. (46) as the intermediate states to calculate $G_{\nu\nu}^>$. If one focuses on the f^1 -peak in the $U \rightarrow \infty$ limit, only the state $|\nu\rangle = \psi_{\nu}^{\dagger}|0\rangle$ plays a role, and one obtains

$$G_{\nu\nu}^>(z) \approx \frac{1 - n_f}{z + \Delta E_0 - \varepsilon_f} = \frac{1 - n_f}{z - \delta}. \quad (47)$$

In this approximation $\rho_{\nu\nu}^>$ has a delta peak at $\varepsilon_f - \Delta E_0 = \delta$. For ε_f well above the Fermi energy $\varepsilon_F = 0$ one has $n_f \ll 1$, and $|\Delta E_0|$ is small compared to ε_f . This leads to a Delta peak of weight ≈ 1 close to ε_f . This is the atomic limit of the trivial empty-level case. Lowering ε_f lowers the peak position but it stays above the Fermi energy. For ε_f well below the Fermi energy the peak is very close to the Fermi energy as $\delta/\tilde{\Delta}$ is exponentially small in $\pi\tilde{\varepsilon}_f/\Delta$ (see Eq. (32)). As $1 - n_f \ll 1$, the weight of the peak is very small. In fact, in this approximation the Kondo peak has zero width.

Obviously when using this leading order description for the calculation of $\rho_{\nu\nu}^<$, the condition $\rho_{\nu\nu}^<(0) = \rho_{\nu\nu}^>(0)$ is not fulfilled. In order to achieve this, one has to go one order higher in $1/N_f$ for the intermediate states inserted in Eq. (45). For ε_f well above the Fermi level, the state $|\nu\rangle$ decays into states $|E\nu\rangle \equiv \psi_{E\nu}^{\dagger}|0\rangle$ with $E \approx \varepsilon_f$, which leads to a peak with a half-width $\pi V(\varepsilon_f)^2 = \pi\tilde{V}(\varepsilon_f)^2/N_f$. The states $|E\nu\rangle$ couple to the states $|E\varepsilon\nu\rangle \equiv \sum_{\nu'} \psi_{E\nu}^{\dagger}\psi_{\nu'}^{\dagger}\psi_{\varepsilon\nu'}|0\rangle/\sqrt{N_f}$ with a matrix element $\tilde{V}(\varepsilon)$, i.e., of order $(1/N_f)^0$. In the infinite- U case these are the additional states to be included. The calculation is similar to the leading-order calculation for $G_{\nu\nu}^<$ presented in the previous subsection but using the inversion formula (40) twice. It leads to [9, 10]

$$G_{\nu\nu}^>(z) = \frac{1 - n_f}{z + \Delta E_0 - \varepsilon_f - \mu(z)} \quad (48)$$

with $\mu(z) = \int_0^B \frac{V(E)^2}{z + \Delta E_0 - E + \tilde{\Gamma}(-z - \Delta E_0 + E + \varepsilon_f)} dE.$

The additional term \tilde{I} in the denominator of the integrand of $\mu(z)$ results from including the states $|E\varepsilon\nu\rangle$ with a hole in the conduction band. Neglecting \tilde{I} gives the result for the width of the peak near ε_f well above the Fermi energy, mentioned above. For ε_f well below the Fermi energy it is essential to include \tilde{I} . Then the integrand on the right-hand side has a pole at $z = E$ of strength $1 - n_f$ leading to $-\text{Im } \mu(\varepsilon + i0) = (1 - n_f)\pi V(\varepsilon)^2$. This leads to

$$\rho_f^>(\varepsilon) = \frac{(1 - n_f)^2 \tilde{V}(\varepsilon)^2}{(\varepsilon - \delta - \text{Re } \mu(\varepsilon))^2 + ((1 - n_f)\pi V(\varepsilon))^2} \quad \text{for } 0 \leq \varepsilon \leq \delta. \quad (49)$$

In a strict $1/N_f$ expansion of $\rho_f^>$, the contributions from μ in the denominator are of order $1/N_f$ and can be neglected. With this assumption $\rho_f^>(\varepsilon)$ joins smoothly to the low-energy result $\rho_f^<(\varepsilon)$ in Eq. (44). The steep rise found there for $-\delta \leq \varepsilon \leq 0$ continues for $\rho_f^>(\varepsilon)$. In the region $\varepsilon \approx \delta$ the strict $1/N_f$ expansion fails, and the full expression in Eq. (49) has to be used. This gives the Kondo peak a half-width $(1 - n_f)\pi V(\delta)^2 \approx \pi n_f \delta / N_f$. The correct treatment of the energy range $\varepsilon \geq \delta$ within the approximation given by Eq. (48) requires the inclusion of the ‘‘continuum part’’ of μ . Unfortunately the approximation Eq. (48) for $G_{\nu\nu}^>$ leads to an additional weak, unphysical pole slightly below $\varepsilon = 0$. A different type of anomaly appears in the NCA at zero temperature [57]. For large N_f , the NCA properly describes how the weight of the Kondo resonance decreases with increasing T , where the scale is given by the Kondo temperature.

One can summarize the behavior of the f^1 peak as a function of ε_f as follows: Lowering ε_f from well above the Fermi energy to well below it, its position goes from ε_f very close to $\varepsilon_F = 0$ to its weight $(1 - n_f)N_f$ and width $(1 - n_f)\pi \tilde{V}(\delta)^2 / N_f$ is reduced as n_f goes from ≈ 0 to ≈ 1 .

For a comparison with experiment, it is crucial to take into account that U is finite, since this leads to a second f^2 -like peak in the BIS spectrum. Using the leading-order, finite- U ground state and additional intermediate states with a doubly occupied f level and a hole in the conduction band, the resulting matrix has to be inverted numerically [10, 11]. The f^2 peak has a broadening of 2Δ (half-width), as the f^2 state can decay by the hopping of either of the two f electrons into the conduction band. It shows a tailing towards higher energies. The reason is that the intermediate states with two electrons in the f level have a hole in the conduction band. This hole is likely to be close to the Fermi energy but can also be located further down.

In the spin-degenerate case $N_f = 2$ a half-filled symmetric band and $2\varepsilon_f + U = 0$ lead to particle-hole symmetry and the Kondo resonance is at $\varepsilon = 0$ as shown in Fig. 1. For $N_f > 2$ the Kondo resonance is above the Fermi level for $2\varepsilon_f + U = 0$ [24]. In order to obtain the Kondo resonance exactly at $\varepsilon = 0$ for $N_f = 2$ an infinite summation of skeleton diagrams in the generating functional is necessary leading to the symmetrized finite- U NCA [25].

Let us summarize the behavior of the total spectral function $\rho_f = \rho_f^< + \rho_f^>$ in the Kondo regime $-\varepsilon_f \gg \tilde{\Delta}$ for large values of U : The ionization peak near ε_f has weight $n_f \approx 1$; the weight of the f^1 peak (Kondo peak) slightly above ε_F is $(1 - n_f)N_f$, and the f^2 peak near $\varepsilon_f + U$ has a weight $n_f(N_f - 1) \approx N_f - 1$. Therefore, even for $n_f = 0.9$ and $N_f = 14$, the weight of the f^1 peak is higher than that of the ionization peak. Despite the fact that there is a small chance, $1 - n_f$, to find the f level empty, there are N_f different ways to place the electron. The weight of the Kondo peak in the BIS spectrum is a factor N_f larger than the part seen in photoemission.

4.3 Spectra involving core holes

As mentioned in section 2.2, core-level XPS and X-ray absorption spectroscopy provide additional information about the valence electrons. The Hamiltonian used to describe core-level spectra of mixed-valence systems takes the form presented in Eq. (17) with $U_{dc} \rightarrow U_{fc}$ and H_A replaced by the valence Hamiltonian H of Eq. (21). With the assumptions explained in section 2.2 the core spectral function is given by

$$\rho_c(\varepsilon) = \left\langle E_0(N) \left| \delta(\varepsilon - \varepsilon_c - E_0(N) + \tilde{H}) \right| E_0(N) \right\rangle, \quad (50)$$

where \tilde{H} is the Hamiltonian of Eq. (21) with ε_f replaced by $\tilde{\varepsilon}_f \equiv \varepsilon_f - U_{fc}$. In the infinite- U case to order $(1/N_f)^0$ the ground state is given by Eq. (29), and the states $|0\rangle$ and $|\varepsilon\rangle$ defined in Eq. (23) are used as intermediate states in the calculation of $G_{cc} = G_{cc}^<$. The matrix elements $\tilde{H}(z)_{ij} \equiv \langle i | (z + \tilde{H} - E_0(N)) | j \rangle$ are easily written down. The $00, 0\varepsilon, \varepsilon 0$ and $\varepsilon\varepsilon'$ matrix elements of the inverse matrix $\tilde{H}(z)^{-1}$ are all needed. The calculation is analogous to obtaining the Green's functions of a noninteracting Anderson model. With $\tilde{z} \equiv z - \varepsilon_c - \Delta E_0$, this yields e.g., $(\tilde{H}(z)^{-1})_{00} = (\tilde{z} - \tilde{\Gamma}(\tilde{z} + \tilde{\varepsilon}_f))^{-1}$ with $\tilde{\Gamma}$ defined in Eq. (42). After some algebra [9], the result can be brought into the form

$$\rho_c(\varepsilon + \varepsilon_c) = (1 - n_f) \left(\frac{U_{fc}}{\varepsilon - U_{fc}} \right)^2 \tilde{\rho}_f(\varepsilon - \Delta E_0 + \varepsilon_f - U_{fc}), \quad (51)$$

where

$$\tilde{\rho}_f(\varepsilon) = -\frac{1}{\pi} \text{Im} \frac{1}{\varepsilon + i0 - \varepsilon_f + U_{fc} - \tilde{\Gamma}(\varepsilon + i0)}. \quad (52)$$

The same type of expression is obtained in the exact solution of the $N_f = 1$ *filled band model* [58]. In this leading order in $1/N_f$ approximation, the core spectrum is directly related to the valence spectrum $\tilde{\rho}_f$. This clearly shows that core-level spectroscopy gives information about properties of the valence electrons, like n_f, ε_f , and Δ . The multiplying factor $[U_{fc}/(\varepsilon - U_{fc})]^2$ changes the weights in $\tilde{\rho}_f$ but does not normally introduce new structures.

To test the accuracy of the $1/N_f$ method one can study the limit $N_f = 1$, where the exact solution can be obtained by solving the Nozières-de Dominicis integral equation [46] numerically. A comparison of the $1/N_f$ result including the states $0, a, c$, and d in Fig. 2 is shown in Fig. 4. As mentioned in section 2.2 the exact result has an infrared singularity at threshold which is not present in the $1/N_f$ result. To mimic lifetime broadening, the spectra shown were given a Lorentzian broadening of 2Γ (full-width half-max). Despite the fact that the $1/N_f$ calculation includes at most two holes, the asymmetry of the exact solution, which includes an infinite number of electron-hole pairs, is quite well described except very close to threshold.

X-ray absorption spectroscopy of $3d \rightarrow 4f$ transitions has formal similarities with inverse photoemission, as an electron is added to the f -level. The difference is that the final state has the core hole present. The theoretical description therefore, as in core-hole XPS, has to use the Hamiltonian \tilde{H} with $\varepsilon_f \rightarrow \varepsilon_f - U_{fc}$. If one works to lowest order in $1/N_f$, it is possible to obtain an analytical solution even if f^2 configurations are included [9].

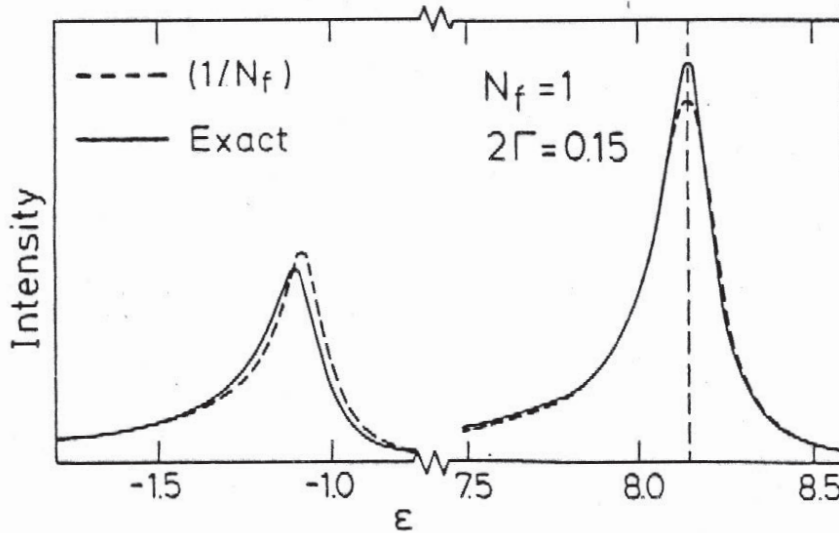


Fig. 4: The core-level spectrum for $N_f = 1$, $\varepsilon_f = 0$, $\Delta = 1.5$, and $U_{fc} = 9$ and a semi-elliptical form of $V(\varepsilon)^2$ with $B = 3$. The spectra are shown with a Lorentzian broadening (FWHM) of 0.15: exact result (full line), using the states 0, a, c, and d of Fig. 2 as intermediate states (dashed line)

5 Comparison with experiment

Model calculations for spectra using the impurity model are frequently used for a comparison with experimental data of lanthanide materials. An example for systems with essentially zero f occupancy in the ground state are La compounds. In Ce systems f^0 and f^1 play the important role. Even in dense systems spectra calculated by the intermediate states method for the Anderson impurity model are often in good agreement with experiment [9, 10, 12, 59]. Switching from the number of electrons in the f level to the number of holes, the formalism presented is easily extended to also describe Yb compounds, as there f^{13} and f^{11} play the same role as the f^1 and f^0 configurations in Ce compounds [54]. To study, e.g., Pr or Nd compounds, the model used here should be generalized.

As the *ab-initio* determination of parameters of model Hamiltonians is a problematic issue, one alternatively adjusts them to experimental data. If, e.g., different spectroscopies are used, a part of the data may suffice to obtain the parameters by fitting to peak positions and their widths. Then additional data can be used as a consistency check. If this turns out to be satisfying for a class of materials, the use of the model in conjunction with a first set of data has predictive power for further measurements. This is what in fact happened with spectra of mixed-valence systems [1]. As an example let us take core-level spectra. The leading peak in Fig. 4 corresponds to final states of mainly f^1 character, while the satellite corresponds to f^0 -like states. These are the important final states for La compounds. For Ce compounds it is important to also take f^2 configurations into account. The core spectrum often has three peaks, corresponding to f^0 , f^1 and f^2 states. The parameters are usually such that the high-energy f^2 peak (shoulder) has a small but observable weight that strongly depends on the value of the coupling parameter Δ [10] and is therefore suitable for its determination.

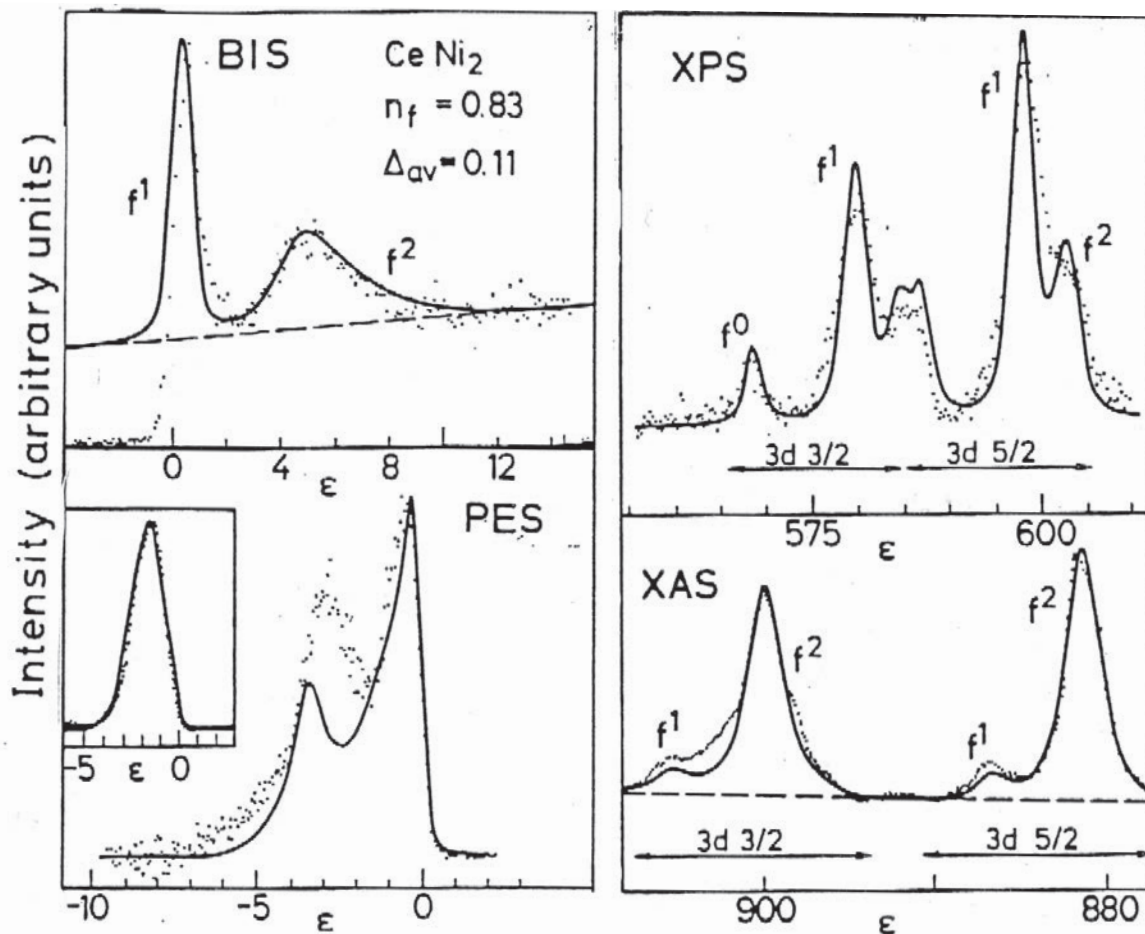


Fig. 5: Comparison of experimental spectra (dots) for $CeNi_2$ with theoretical results using the impurity model. The results for inverse photoemission (BIS), valence photoemission (PES), 3d X-ray photoemission (XPS), and 3d \rightarrow 4f X-ray absorption (XAS) are discussed in the text.

Fig. 5 shows as an example experimental spectra for $CeNi_2$ and the attempts to fit them with a single set of parameters using the Anderson impurity model and the methods discussed in section 4. As the energy dependence of $V(\epsilon)^2$ has to be taken into account [12], the average value Δ_{av} of $\pi V(\epsilon)^2$, extracted from 3d \rightarrow 4f X-ray absorption spectra, $\Delta_{av} = 0.11$ eV is presented. The total f occupancy is inferred to be $n_f = 0.83$. The two components of the XAS spectrum in the figure are due to transitions from the spin-orbit-split 3d 3/2 and 3d 5/2 levels. Each component shows an f^1 and f^2 peak with multiplet structure. The relative weights of the 3d 3/2 and 3d 5/2 components were adjusted to the experiment and a weak background was added as shown. A Lorentzian broadening (FWHM=2.0 eV) was used to describe life-time broadening and instrumental resolution. The parameters obtained from the 3d XPS spectrum differ only slightly from the ones from the XAS data. The f^2 and f^1 -Kondo peak of the shown BIS spectrum were obtained using these parameters. Using the same parameters, the valence-band PES spectrum shows the onset of the Kondo peak at energies close to zero. The peak at $\epsilon \approx -3$ eV is somewhat too low in energy and too narrow ($\epsilon_f = -1.6$ eV was used). Introducing different features in $V(\epsilon)^2$ allows one to improve the agreement with experiment [12]. More information

about the Coulomb parameters used can be found in Ref. [12]. It should be mentioned that for CeNi_2 and other Ce compounds the calculation of the static magnetic susceptibility with the parameters from spectroscopy leads to results in good agreement with the measured values.

As mentioned, there were many theoretical developments in the last thirty years that go beyond the methods presented in sections 3 and 4. The intermediate states method nevertheless has remained a valuable tool in the hands of experimentalists.

Acknowledgements

The author would like to thank Olle Gunnarsson for the critical reading the manuscript and useful suggestions. He originally had come up with the idea of the type of $1/N_f$ expansion presented here, which we then worked on together.

References

- [1] For an earlier review see the articles in: *Handbook on the Physics and Chemistry of Rare Earths*, Vol. 10, *High Energy Spectroscopy*, K.A. Gschneider, L. Eyring, and S. Hufner (eds.), (North Holland, 1987)
- [2] P.W. Anderson, *Phys. Rev.* **124**, 41 (1961)
- [3] A.A. Abrikosov, *Physics* **2**, 5 (1965)
- [4] H. Suhl, *Phys. Rev.* **138**, A515 (1965)
- [5] K. Yamada, *Prog. Theor. Phys.* **53**, 970 (1975)
- [6] T.V. Ramakrishnan, *Perturbative theory of mixed valence systems*, in: *Valence Fluctuations in Solids*, L.M. Falicov, W. Hanke and M.B. Maple (eds.), (North-Holland, 1982);
T.V. Ramakrishnan and K. Sur, *Phys. Rev. B* **26**, 1798 (1982)
- [7] P.W. Anderson, Summary talk, in *Valence Fluctuations in Solids*, L.M. Falicov, W. Hanke and M.B. Maple (eds.), (North-Holland, 1982)
- [8] O. Gunnarsson and K. Schönhammer, *Phys. Rev. Lett.* **50**, 604 (1983)
- [9] O. Gunnarsson and K. Schönhammer, *Phys. Rev. B* **28**, 4315 (1983)
- [10] O. Gunnarsson and K. Schönhammer,
Many-Body Formulation of Spectra of Mixed Valence Systems, in [1]
- [11] O. Gunnarsson and K. Schönhammer, *Phys. Rev. B* **31** 4815, (1985)
- [12] J. Allen *et al.*, *Advances in Physics* **35**, 275 (1986)
- [13] Y. Kuramoto, *Z. Phys. B* **53**, 37 (1983)
- [14] H. Keiter and G. Czycholl, *J. Magn. and Magn. Mater.* **31**, 477 (1983)
- [15] N. Grewe, *Z. Phys. B* **52**, 193 (1983)
- [16] P. Coleman, *Phys. Rev. B* **29**, 3035 (1984)
- [17] H. Keiter and J.C. Kimball, *Int. J. Magn.* **1**, 233 (1971)
- [18] S.E. Barnes, *J. Phys. F* **6**, 1375 (1976)
- [19] K. Wilson, *Rev. Mod. Phys.* **47**, 773 (1975)
- [20] H.O. Frota and L.N. Olivera, *Phys. Rev. B* **33**, 7871 (1986)
- [21] for a review see: R. Bulla, T.A. Costi, and T. Pruschke, *Rev. Mod. Phys.* **80**, 395 (2008)

- [22] J. Holm and K. Schönhammer, *Solid State Commun.* **69**, 969 (1989)
- [23] T. Pruschke and T. Grewe, *Z. Phys.* **74**, 439 (1989)
- [24] J. Holm, R. Kree and K. Schönhammer, *Phys. Rev. B* **48**, 5077 (1993)
- [25] H. Haule, S. Kirchner, J. Kroha, and P. Wölfle, *Phys. Rev. B* **64**, 155111 (2001)
- [26] S. Kirchner, J. Kroha, and P. Wölfle, *Phys. Rev. B* **70**, 155301 (2004)
- [27] D.E. Logan, M.P. Eastwood, and M.A. Tusch, *J. Phys. Condens. Matter* **10**, 2673 (1998)
- [28] M.R. Galpin, A.B. Gilbert, and D.E. Logan, *J. Phys. Condens. Matter* **21**, 375602 (2009)
- [29] P.W. Wiegmann, *Phys. Lett. A* **80**, 163 (1980)
- [30] N. Kawakami and A. Okiji, *Phys. Lett. A* **86**, 483 (1981)
- [31] P. Schlottmann, *Phys. Rev. Lett.* **50**, 1697 (1983)
- [32] W. Metzner and D. Vollhardt, *Phys. Rev. Lett.* **62**, 324 (1989)
- [33] D. Newns, *Phys. Rev.* **178**, 1123 (1969)
- [34] D.N. Zubarev, *Sov. Phys. Usp.* **3**, 320 (1960)
- [35] F. Reinert et al., *Phys. Rev. Lett.* **87**, 106401 (2001)
- [36] K.O. Friedrichs, *Comm. Pure and Appl. Math.* **1**, 361 (1948)
- [37] T.D. Lee, *Phys. Rev.* **95**, 1329 (1954)
- [38] K. Yoshida and K. Yamada, *Prog. Theor. Phys.* **53**, 1286 (1975)
- [39] W. Brenig and K. Schönhammer, *Z. Phys. B* **267**, 201 (1974)
- [40] A.C. Hewson, *Phys. Rev.* **144**, 120 (1966)
- [41] A. Theumann, *Phys. Rev.* **178**, 120 (1969)
- [42] C. Lacroix, *J. Phys. F***11**, 2389 (1981)
- [43] S.-J. Oh and S. Doniach, *Phys. Rev. B* **26**, 2085 (1982)
- [44] G. Czycholl, *Phys. Rev. B* **31**, 2867 (1985)
- [45] A. Hewson, *The Kondo Problem to Heavy Fermions*, (Cambridge University Press, 1993)
- [46] P. Nozières and C.T. de Dominicis, *Phys. Rev.* **178**, 1097 (1969)
- [47] P.W. Anderson, *Phys. Rev. Lett.* **18**, 1049 (1967)

- [48] M. Combescot and P. Nozières, *J. de Physique* **32**, 913 (1971)
- [49] A. Kotani and Y. Toyozawa, *J. Phys. Soc. Japan* **35**, 563 (1974); **35**, 912 (1974)
- [50] K. Schönhammer and O. Gunnarsson, *Solid State Commun.* **23**, 691 (1977)
- [51] K. Schönhammer and O. Gunnarsson, *Solid State Commun.* **26**, 399 (1978)
- [52] K. Schönhammer and O. Gunnarsson, *Phys. Rev. B* **18**, 6606 (1978)
- [53] C.M. Varma and Y. Yafet, *Phys. Rev. B* **13**, 2950 (1976)
- [54] N.E. Bickers, D.L. Cox, and J.W Wilkins, *Phys. Rev. Lett.* **54**, 230 (1985)
- [55] F. Patthey, B. Delley, W.-D. Schneider, and Y. Baer, *Phys. Rev. Lett.* **55**, 1518 (1985)
- [56] L. Hedin and S. Lundqvist, in *Solid State Physics*, Vol. 23,
H. Ehrenreich, D. Turnbull, and F. Seitz (eds.), (Academic Press, New York, 1969)
- [57] E. Müller-Hartmann, *Z. Phys.* **57**, 281 (1984)
- [58] K. Schönhammer and O. Gunnarsson, *Z. Phys. B* **30**, 297 (1978)
- [59] Y. Baer and W.-D. Schneider,
High-Energy Spectroscopy of Lanthanide Materials – an Overview, in [1]

